European Journal of Clinical Pharmacy
Print ISSN: 2385-409X **Online ISSN**: Applied Website:
https://farmclin.com/

Impact of a Fractal Function on the Partially Coherent Laser Beam in Biological Tissues

Abdulrazak Abdulsalam Mohammed[1], Faroq Saad[1], Safaa Mustafa Hameed[2]

[1]Department Of Radiological Imaging Technologies, Cihan University-Erbil, Erbil, Kurdistan Region, Iraq

[2]Department of Optics Technologies, College of Health & Medical Technology, Sawa University, Almuthana, Iraq.

ABSTRACT

Absorption primarily governs the biological effect of laser light. The tissue converts photon energy into heat which results in an increase of the tissue's internal temperature. One is a cosin-type intensity pattern including Fraunhofer conditions bracketed by this function. A partially coherent generic fractal element is examined to illustrate laser beam propagation throughout various biological tissues in addition to several cases relating to the parameters of partly cohesive fractal elements. Results and Discussion — We numerically investigate the impact of the fractal function on the output laser beam. The results of this investigation may find applications in imaging technology and medical diagnostics.

KEYWORDS: Partially coherent laser beam; Fractal function; Biological tissue.

How to Cite: Abdulrazak Abdulsalam Mohammed, Faroq Saad, Safaa Mustafa Hameed, (2026) AImpact of a Fractal Function on the Partially Coherent Laser Beam in Biological Tissues ., European Journal of Clinical Pharmacy, Vol.8, No.1, pp. 2599-2617

INTRODUCTION

Recently, researchers conducted a comprehensive study of a beam traversing a medium of soft tissue utilizing a power spectrum model [1,2] and the fractal function method [3,4]. The interaction of light beams with biological tissue has recently garnered significant attention for enhancing tissue imaging technology through optical coherence tomography (OCT) in disease diagnosis. Research into the changing characteristics of laser beam propagation through tissue media is valuable for enhancing the quality of diagnostic and imaging procedures [8]. Numerous studies in the literature have examined various beam intensity patterns. Since that time, researchers have investigated the effects of partial coherence on beam propagation within tissue media. Researchers have conducted evaluations of the structure of biological tissue by analyzing the spreading beam and the distribution of the Gaussian-Schell model [9]. Lu et al. [10] have investigated the influence of biological tissue on anomalous hollow beams. Furthermore, researchers have examined the intensity pattern of a hollow Gaussian beam within a biologically-derived tissue medium [11]. Comparable findings apply to partially coherent Lommel-Gaussian and rectangular multi-Gaussian beam models, while coherent Laguerre-Gaussian and vortex beams have been demonstrated within the same tissue medium [12-16]. Additionally, further research has been conducted regarding the index of scintillation and the distribution of beam intensity in tissue media [17, 18].

By studying the polarization profile and also the spatial characteristics of scattered beams researchers have evaluated interaction of light-beams with tissue-mimicking phantoms [19]. The Hermite-Sinusoidal-Gaussian (HSG) mode solution derived by Casperson and Tovar for a class of light beams provides insights into frame-symmetric beam solutions propagating through complex optical systems. The HSG beam can be used to characterize a wide range of light beams including those with sophisticated intensity distributions [21-23]. Specifically, Bayraktar has analyzed the change in magnitude of a partial coherent hyperbolic sinusoidal Gaussian beam as it travels through different types of tissue. Recently, Saad et al. proposed a modified anomalous vortex beam which generated partly coherent vortex in the context of biological tissues [25]. This paper aims to show how the fractal function influences partially coherent beams. The unique features that characterize these types of laser beams have attracted a lot of interest because they provide more use in practice.

PARTIALLY COHERENT BEAM WITH A FRACTAL FUNCTION IN BIOLOGICAL TISSUES

The function of cross-spectral density (CSD) for a partially coherent beam in the input plane is described by [26]:

$$W_0(r_1, r_2, z=0) = A_o^2 \left(\frac{x_1}{\omega_0}\right)^t \left(\frac{x_2}{\omega_0}\right)^t \sinh^n(\Omega x_1) \sinh^n(\Omega x_2) \times \exp\left(-\frac{x_1^2 + x_2^2}{\omega_0^2}\right) H_m\left(\frac{\sqrt{2}}{\omega_0} x_1\right) H_m\left(\frac{\sqrt{2}}{\omega_0} x_2\right) \times \exp\left[-\frac{(x_1 - x_2)^2}{2\sigma_0^2}\right] \times \left(\frac{y_1}{\omega_0}\right)^t \left(\frac{y_2}{\omega_0}\right)^t \sinh^n(\Omega y_1) \sinh^n(\Omega y_2) \times \exp\left(-\frac{y_1^2 + y_2^2}{\omega_0^2}\right) H_m\left(\frac{\sqrt{2}}{\omega_0} y_1\right) H_m\left(\frac{\sqrt{2}}{\omega_0} y_2\right) \exp\left(-\frac{(y_1 - y_2)^2}{2\sigma_0^2}\right), \quad (1)$$

where

$$\sinh^n(t) = \frac{1}{2^n}\sum_{s=0}^{n}(-1)^n \exp(-e_{sn}t) \tag{2}$$

Where sinh n(t) and s0 are coherent parameters esn=(2s-n), where the position vectors at the initial plane are r1=(x1, y1) and r2=(x2, y2), ω0 refers to the radius of the waist, n represents the beam order, l indicates the hollowness parameter, and Hj (.) denotes the jth order of the Hermite polynomials (j=m and u). A0 is the amplitude of the field, and Ω represents the decentered parameters related to the sinh(t).

This value is the coherence parameter. By modulating the laser beam, the term can be expressed as a fractal method [27, 28].

FRACTUAL FUNCTION

A fractal is a disjointed geometric figure that a singular equation cannot describe, yet it demonstrates uniform irregularity across all scales. To characterize an entity such as a laser beam, one would employ the notion of partitioning a whole into miniature, scaled-down replicas. Fractals are generally self-similar, scale-invariant, and display infinite patterns. Fractal patterns may accurately depict a range of real-world items. The essential mathematics and physics of fractal functions encompass two primary variables: length and angle, which relate to scalar and vector ideas. Thus, the fractal dimension (D) may be determined using the subsequent equation [27, 28]:

$$D = \frac{\log(N)}{\log(r)}, \tag{3}$$

In this context, N signifies the quantity of boxes that encompass the area, whereas r indicates the magnification or the reciprocal of the box size. Fractal dimensions provide insights into the static geometry of an object. Fractal methods may be applied within iterated function systems (IFS). Non-linear deterministic equations can produce irregular outputs autonomously.

Let H(x) & h(d) is a space matrix and f(x) be a function :

$$f(s) = \{f(x) : x \subset s\}, \tag{4}$$

The equation can give the metric space:

$$A' = AT, \tag{5}$$

where A is a point in the initial area.

A' Is a new point in the under matrix operation (T), which is given by

$$T = \begin{pmatrix} a & b \\ c & d \end{pmatrix}, \tag{6}$$

The transform W The Euclidean plane is given by

$$W(x, y) = (ax + by + e, cx + dy + f), \tag{7}$$

In this context, a, b, c, and d are defined as rotation and scaling operators that will be applied to the point, collectively referred to as a fine transformation. Additionally, e and f are points that define the translation to be applied to the point.

$$W(x) = w\begin{pmatrix} x \\ y \end{pmatrix} = \begin{pmatrix} a & b \\ c & d \end{pmatrix}\begin{pmatrix} x \\ y \end{pmatrix} + \begin{pmatrix} e \\ f \end{pmatrix}, \tag{8}$$

then $W(x) = Ax + T$, (9)

where

$$Ax = \begin{pmatrix} a & b \\ c & d \end{pmatrix}\begin{pmatrix} x \\ y \end{pmatrix}, \tag{10}$$

Then T is a horizontal vector

$$T = \begin{pmatrix} e \\ f \end{pmatrix}. \tag{11}$$

Table 1: The parameter values of the above matrix in Eq. (10) can be given as

No.	a	b	c	d	e	f	x	y
1	0.100	0.000	0.000	0.100	2.700	0.000	3.000	0.000
2	0.100	0.000	0.000	0.100	2.184	1.588	2.427	1.674
3	0.100	0.000	0.000	0.100	0.834	2.568	0.927	2.853
4	0.100	0.000	0.000	0.100	-0,834	2.568	-0.927	2.853
5	0.100	0.000	0.000	0.100	-2.184	1.588	-2.427	1.764
6	0.100	0.000	0.000	0.100	-2.700	0,000	-3.000	0.000

7	0.100	0.000	0.000	0.100	-2.184	-1.588	-2.427	-1.764
8	0.100	0.000	0.000	0.100	-0.834	-2.568	-0.927	-2.853
9	0.100	0.000	0.000	0.100	0.834	-2.568	0.927	-2.853
10	0.100	0.000	0.000	0.100	2.184	-1.588	2.427	-1.764

An investigation will be conducted on the propagation of laser beams through soft tissue media using a fractal function, with a focus on the interaction between the light beam and biological tissue for disease diagnosis. The variation in energy, influenced by the fractal pattern, dictates the frequency at which the laser emits light. The radiation emitted $_0$ corresponds to a particular frequency and a defined intensity at each segment of the fractal structure. This indicates that the laser produces radiation at a specific wavelength (λ). The angle characterizes the divergence of the aperture.

$$\theta = \beta \frac{\lambda}{D}, \tag{12}$$

where β It is a factor of proportionality, λ is the wavelength, and D is the diameter of the aperture.

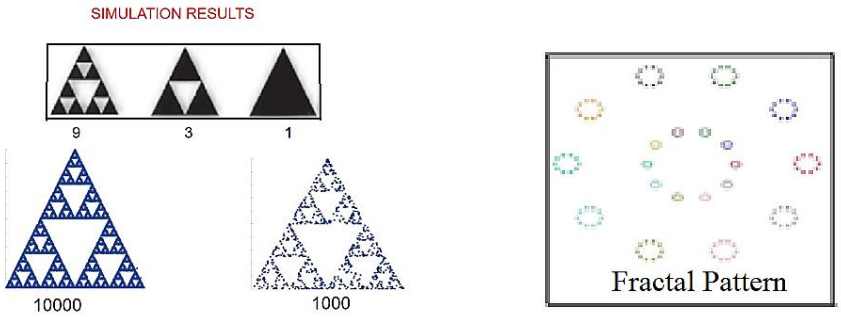

(b)

Fig. 1: (a) Irritation of Fractal elements, (b) Circular distribution of the fractal pattern.

After distributing it in a circular form, a fractal pattern is obtained, and the resulting output frequency is shown in Fig. 2

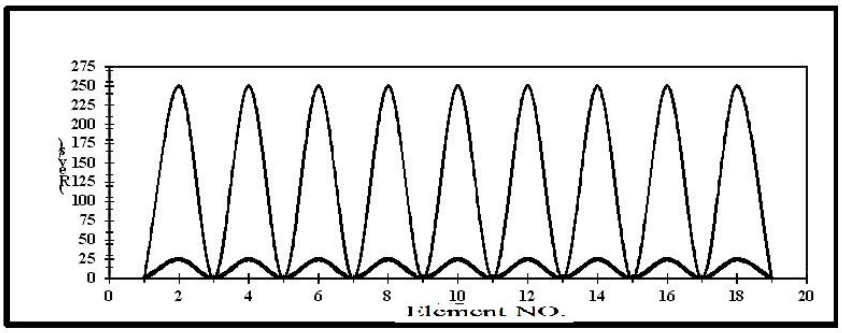

Fig. 2: Numerical aperture (NA) of a laser beam incident on biological tissue by fractal function

Relative aperture = D/f. D is the diameter of the aperture & f focal length.

$$NA = n \sin \theta_{arc}, \tag{13}$$

where n is the refractive index of the medium and θ_{arc} is the arc angle
Eq. (13) can be rewritten as:

$$NA_{fractal} = n \sin\left(\tan - 1\left(2\, fD\right)\right) F\left(x\right), \tag{14}$$

where n is the refractive index and F(α) is the fractal dimension operator. The output spectrum of each wavelength of the laser is shown in the following table

Table 2: Types of lasers (Some medical uses of lasers)

Wavelength	Color
(495nm -570nm)	Green laser
(450nm -495nm)	Blue laser
(620-740nm)	Red laser
(10-400nm)	UV-Laser

(780nm 1mm)	IR-Laser

LASERS

Lasers are now extensively utilized in the field of medicine. A fundamental difference between lasers and other light sources is their narrow spectral width—typically around 1 nm—indicating that the light is produced at a single wavelength. This yields a more focused light output. Thus, a laser functioning at the same nominal power and wavelength as other sources can transmit greater energy to the target.

Lasers operating at the same wavelengths can elicit comparable biological responses, however, with varying degrees of efficacy [29]. Sato et al. demonstrated in their work on near-infrared photoimmunotherapy (NIR-PIT) that laser light was more efficacious in inducing cell death compared to other light types, given equivalent energy exposure, in both flat and spherical cell cultures in the laboratory. Laser light exhibited enhanced therapeutic benefits in vivo during NIR-PIT at an equivalent light dosage in murine models [30]. Furthermore, a constraint is present for specific NIR-PIT applications, especially in oncology, where illumination must be transmitted via catheters, endoscopes, or needles. In such instances, coherent narrow-beam laser light is favored.

LASER INTRATION WITH SKIN:

The skin as discussed above has some certain properties which affect the absorption and penetration of laser light by skin cells. Laser systems work by emitting light that interacts with tissue in a four principal manners: transmission, reflection, scattering and absorption [31]. Absorption is the modulator of the biological action of laser light. When a photon encounters tissue, it transfers energy in this fashion; that is to say, the photon can be reemitted as radiant light or absorbed into heat which increases the internal temperature of such tissue [32, 33, 34]. The flickering of laser light in the skin relies on its interaction with individual chromophores, which are endogenous substances that absorb certain wavelengths. The major endogenous cutaneous chromophores are: water, melanin and hemoglobin [35, 36]. In addition, laser scattering within biological tissue affects light energy intensity [37]. The energy emitted by the laser scales inversely with wavelength. Laser light penetrates biological tissue better at longer wavelengths until the mid-infrared range, where water in the tissues absorbs most of the laser energy. [36]

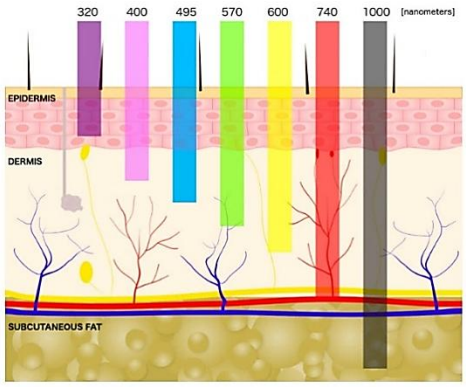

Fig. 3: The skin cross-section showing dermal penetration by different wavelengths of light (in order from the left: UVB, UVA, blue light, green light, yellow light, red light, infrared light).

A deeper understanding of the interaction between lasers and skin enables specialists to choose precise laser parameters in their therapies, including the wavelength of the laser light, intensity, duration of radiation, and density of laser beam energy [38]. Table 2 outlines various medical applications of lasers.

THE UV LIGHT (10-400NM):

Ultraviolet radiation, as one of the main types of non-ionizing radiation emitted by the sun, is essential for life to develop on our planet. It is remarkable that the sun divides UV radiation into three separate ranges, showing different biological effects: UVA (320–400 nm), UVB (280–320 nm) and UVC (200–280 nm). The ozone layer of Earth prevents most UVC radiation from reaching Earth's surface and blocks about 95% of UVB radiation. Part of the UVB rays, which are not absorbed by the ozone layer reach only the surface layers of epidermis and papillary dermis. It is crucial to recognize the harmful outcomes of UVB. In contrast, UVA radiation penetrates and is absorbed more deeply into the dermis layers.

UV lasers classified into three categories. A Q-switched Nd: YAG laser delivers 353 nm ultraviolet (UV) laser irradiation, which is produced experimentally from a lnd=1064nm(infrared) via an appropriate crystal. This second category of lasers is used in psoriatic treatment [43] and adopts gas (excimer) laser. The third type is a metal vapor laser.

Ultraviolet radiation is a well known harmful factor to the skin, causing cell damage and photoaging as well as potential carcinogenic impact [43, 44]. Additionally, skin chromophores absorb radiation or reactive free radicals (reactive oxygen species–ROS) in the interstitial water of the skin leading to premature aging associated with pigmentation changes and a loss of

collagen [44]. Keratinocytes are the most affected cells exposed to ultraviolet radiation in skin and secrete inflammatory cytokines, such as IL-1α, IL-1β and IL-6. Specific and crosslinked cycles of pro inflammatory cytokines induce an increase in matrix metalloproteinase 1 (MMP-1) production and release. The long term effect of UVB inflammatory response is to break down the internal micro-structure of skin due to which skin gets aged faster. Gruber et al.
[44, 45] showed similar skin effects of UVB radiation also in vitro reconstruct human skin model, such as MatTek EpiDerm. Irrespective of these advances, our data altogether suggest the potential of reconstructed skin tissues to be used as an alternative in practical skin tests where the natural skin structure can be preserved.[45].

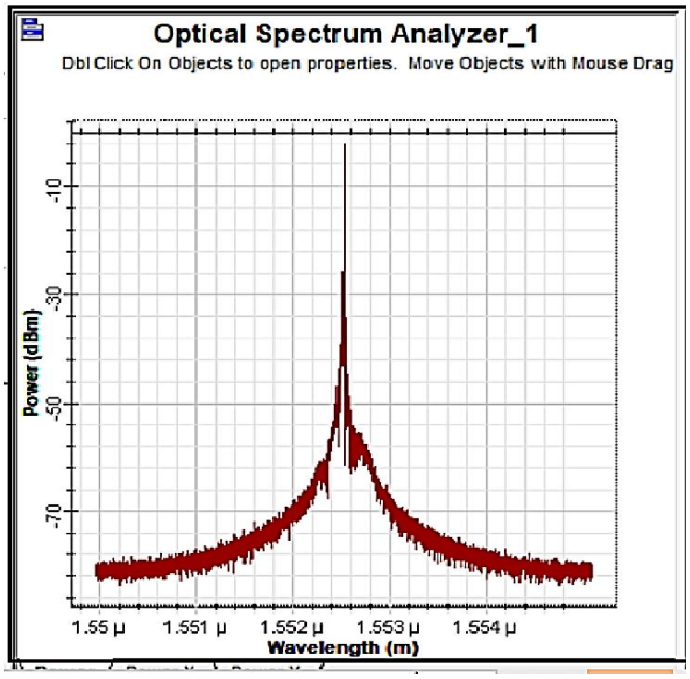

(a) O S A

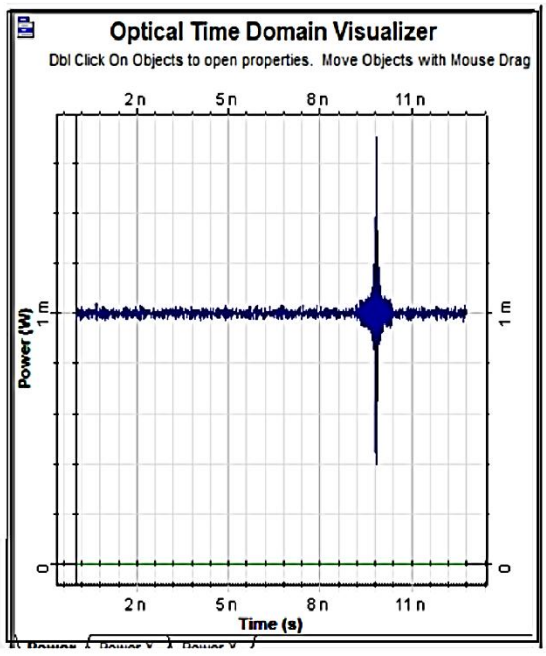

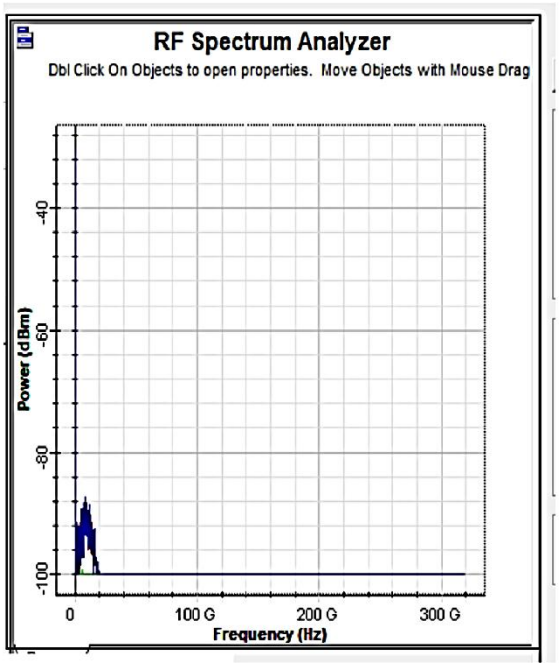

(b) O T D (c) RF- Spectrum Analysis

Fig. 4: OSA, OTD, and RFSA for (400nm) with Fractal method

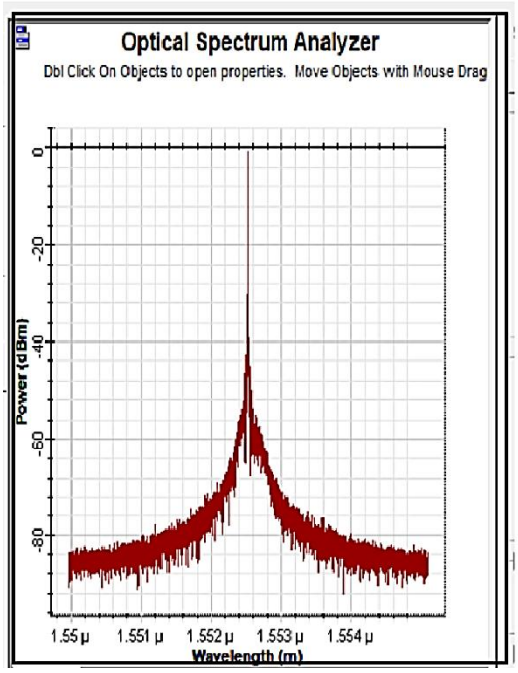

(a) O S A

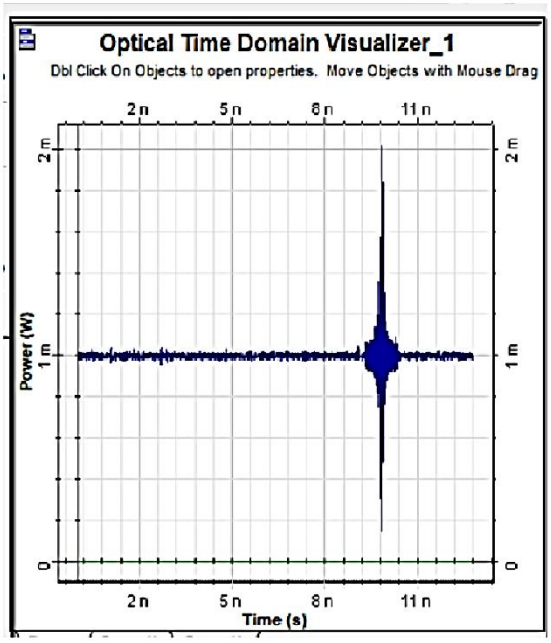

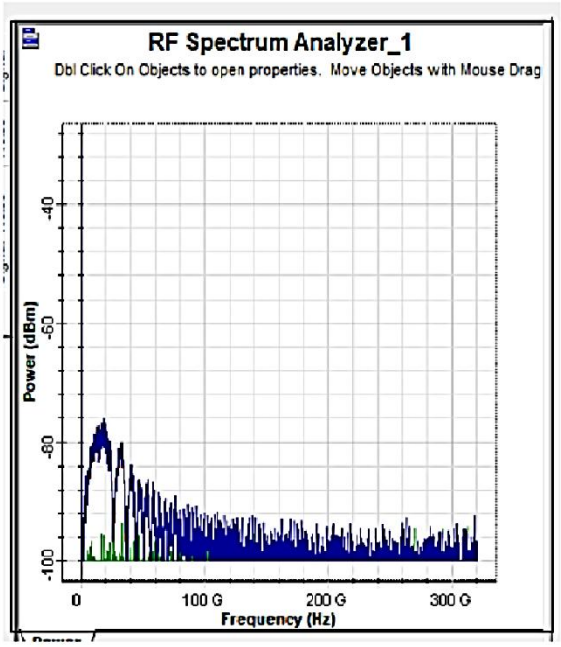

(b) O T D (c) RF-Spectrum Analysis

Fig. 5: OSA, OTD, and RFSA for (400nm) with Normal method

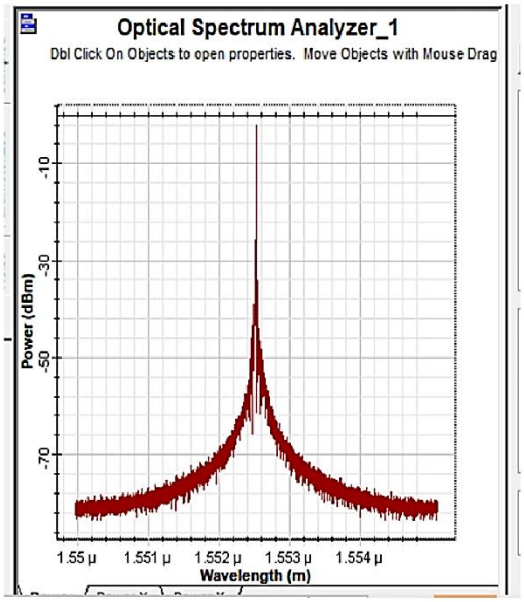

(a) OSA

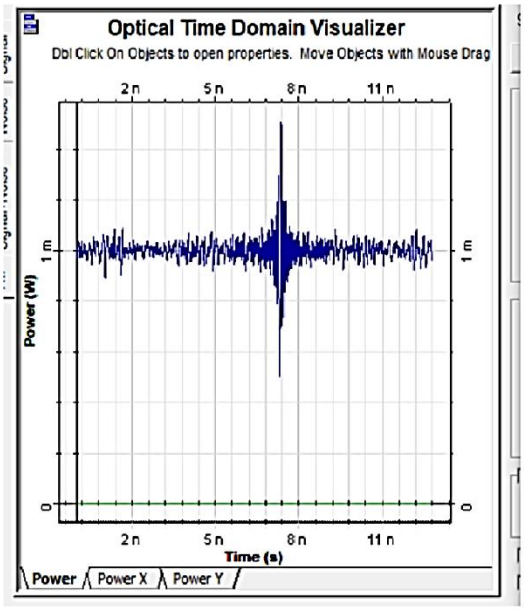

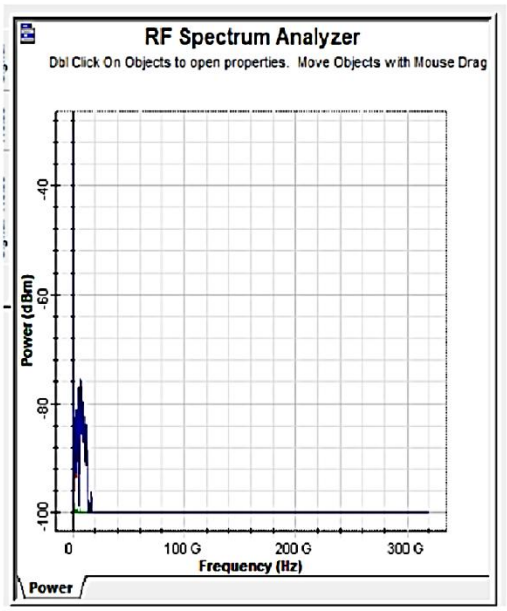

(b)OTD (c) RF-Spectrum Analysis

Fig. 6: OSA, OTD, and RFSA for (740nm) with Fractal method

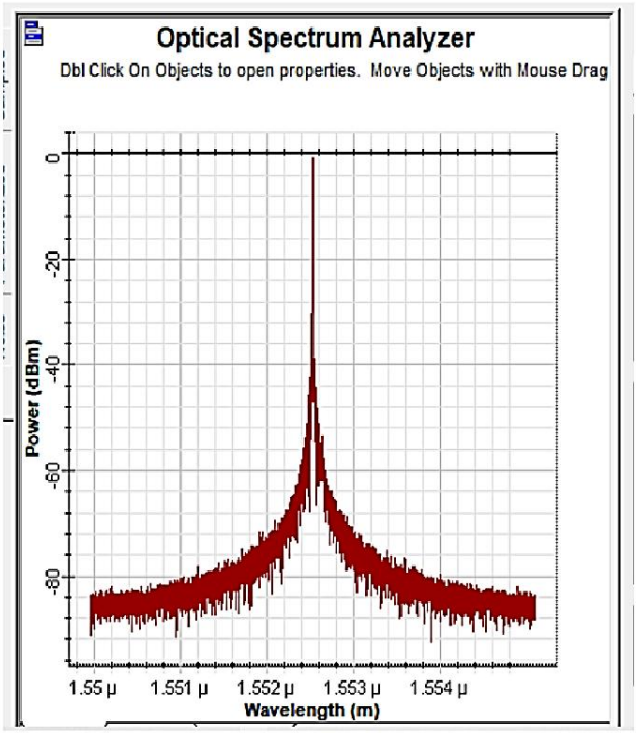

(a)OSA

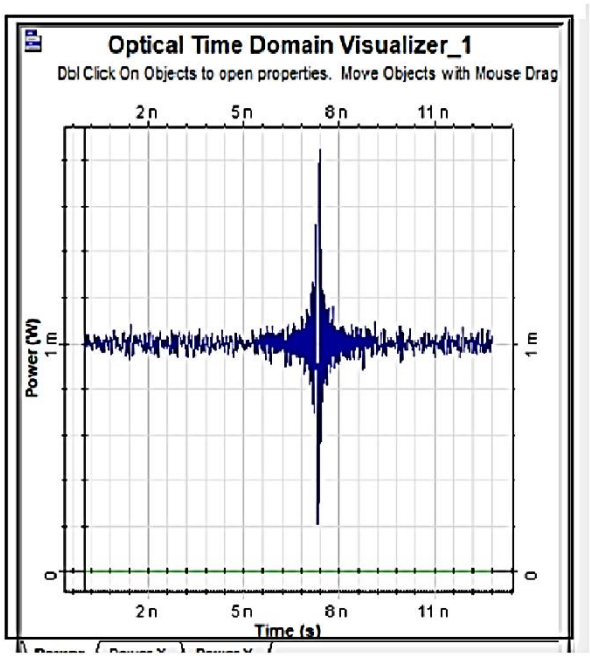

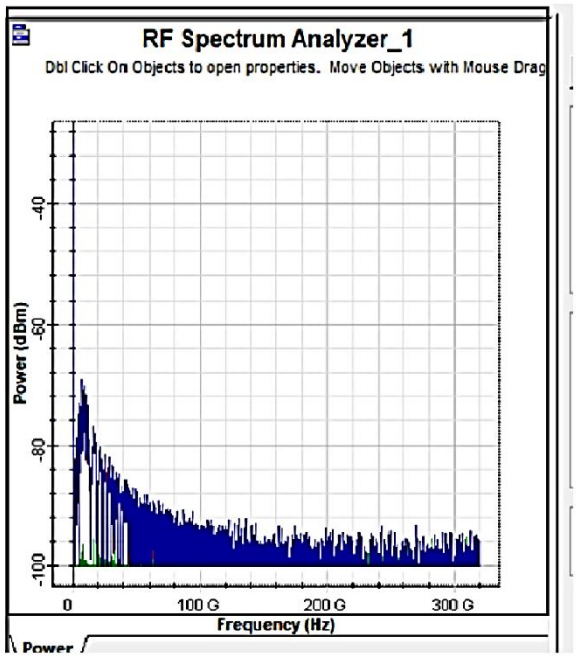

(b)OTD (c)RF-Spectrum analyzer

Fig. 7: OSA, OTD, and RFSA for (740nm)with Normal method

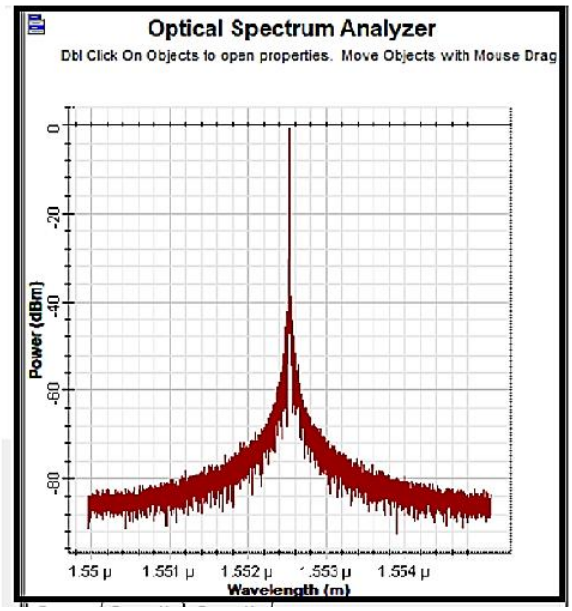

(a)OSA

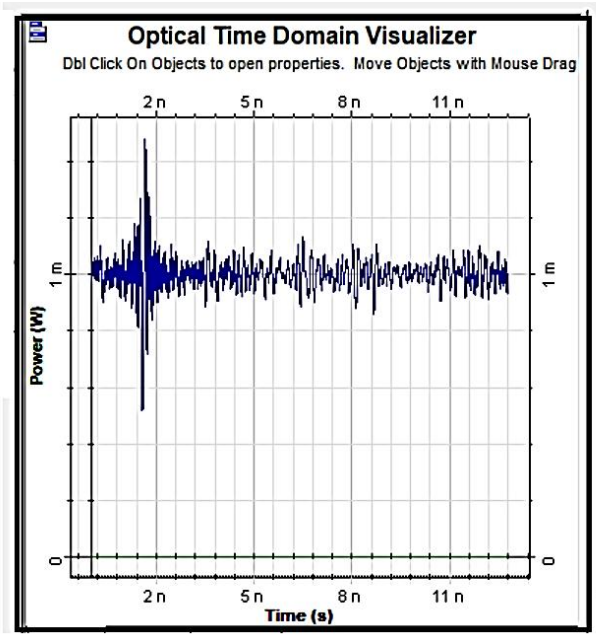

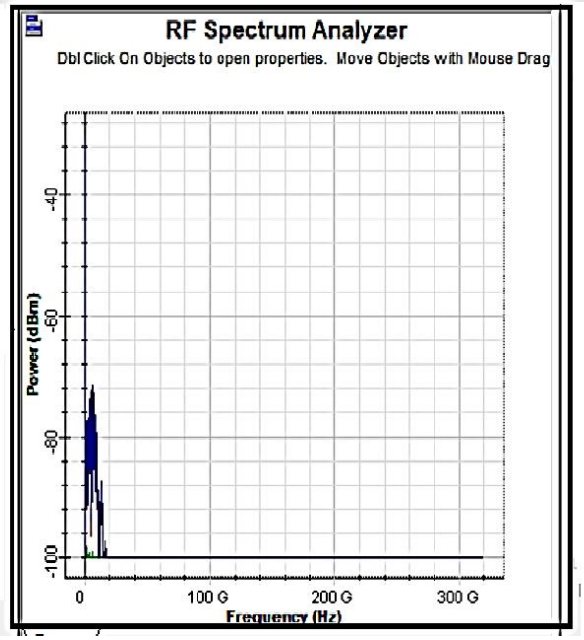

(b)OTD (c)RF-Spectrum Analyzer

Fig. 8: OSA,OTD and RFSA for (1000nm)with Fractal method

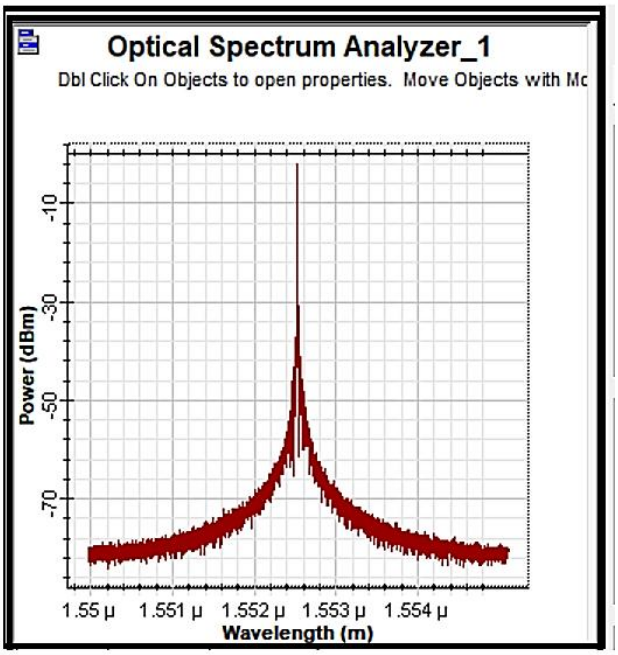

(a)OSA

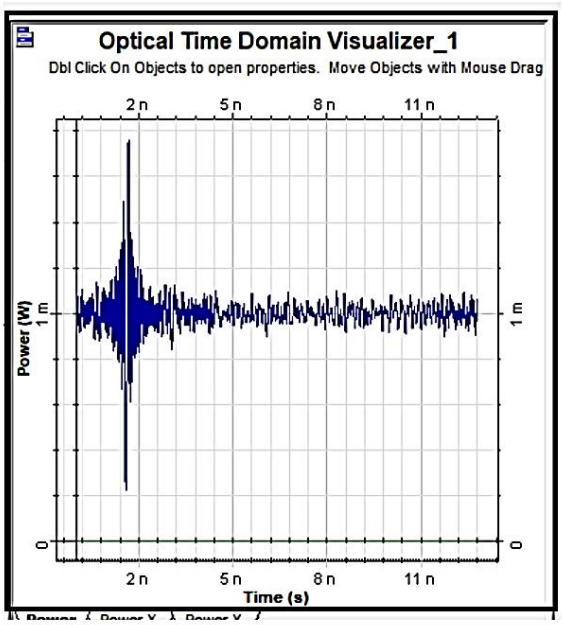

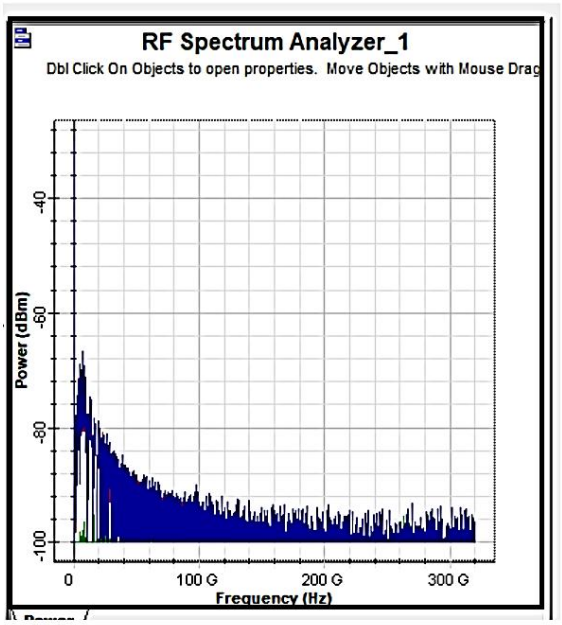

(b)OTD (c)RF-Spectrum Analyzer

Fig. 9: OSA, OTD, and RFSA for (1000nm), with Normal method

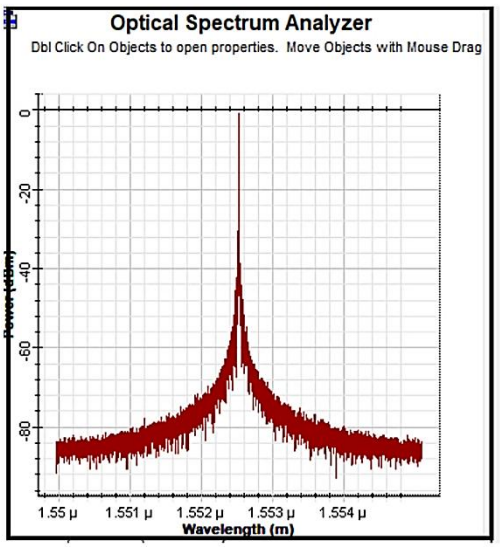

(a) OSA

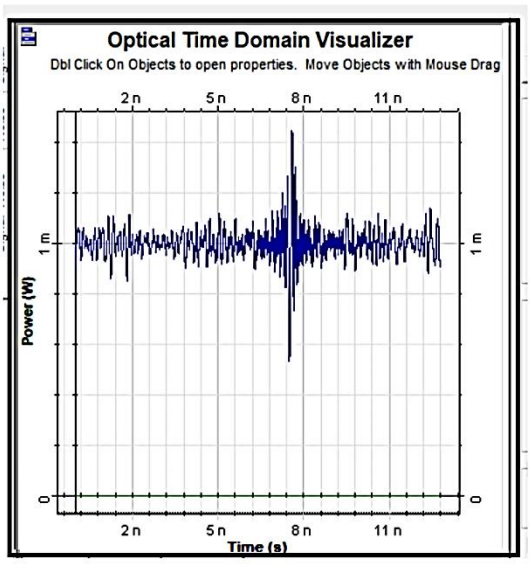

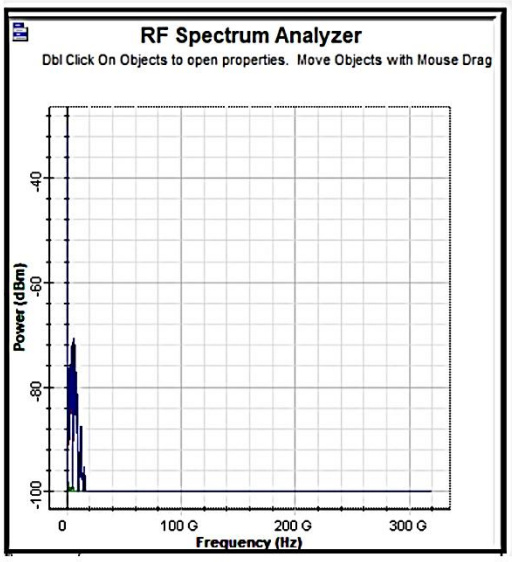

(b)OTD (C)RF-Spectrum Analysis

Fig.10: OSA, OTD, and RFSA for (1150nm) with Fractal method

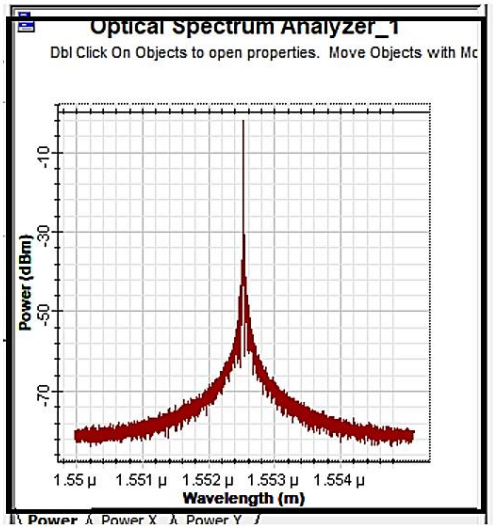

(a)OSA

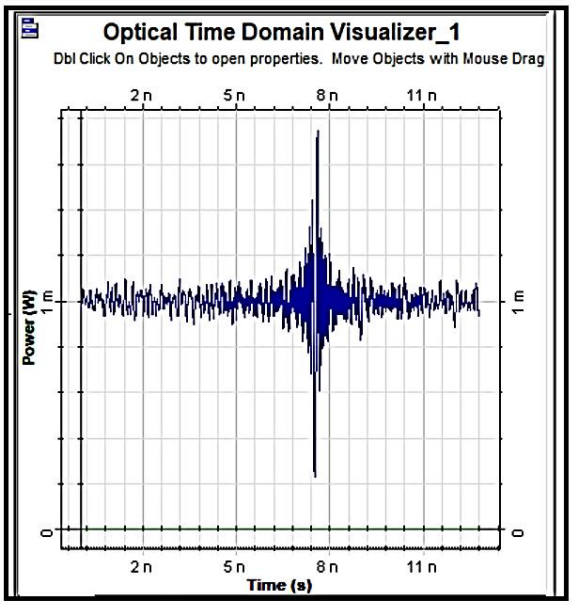

(b)OTD

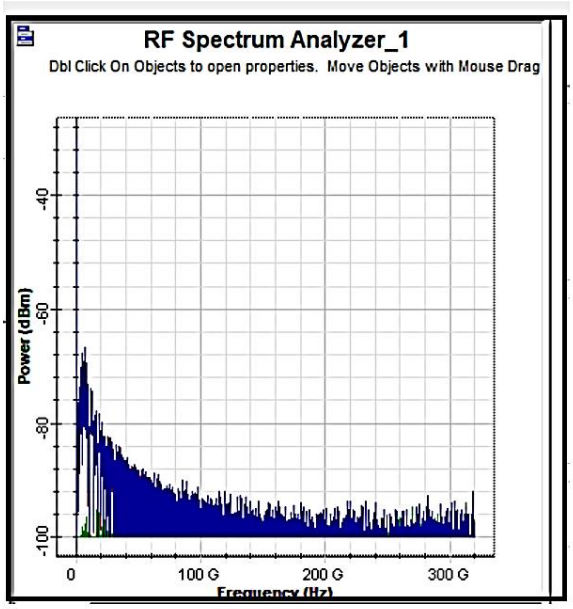

(c)RF-spectrum Analyzer

Fig.11: OSA, OTD, and RFSA for (11500nm) with Normal method

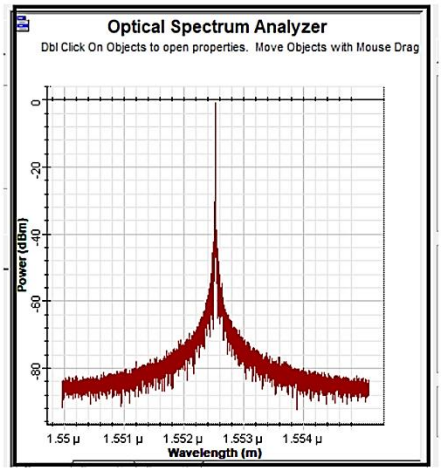

(a)OSA

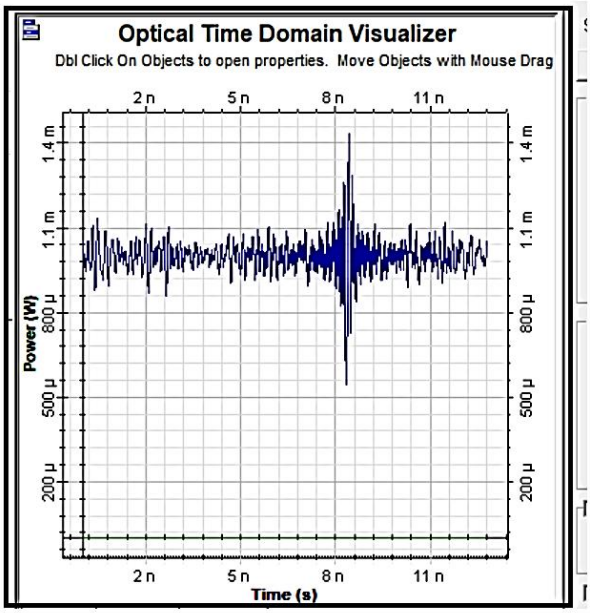

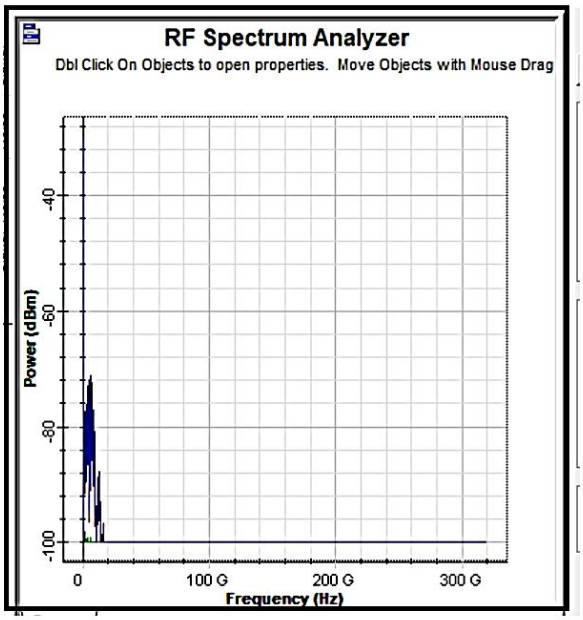

(b)OTD (c)Rf-Spectrum Analyzer

Fig. 12: OSA, OTD, and RFSA for (1400nm)with Fractal method

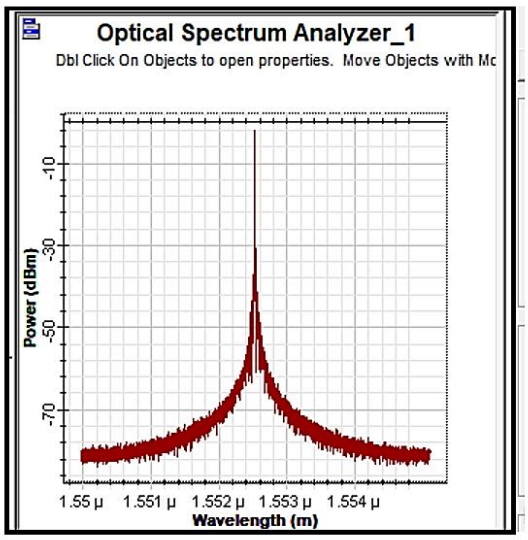

(a)OSA

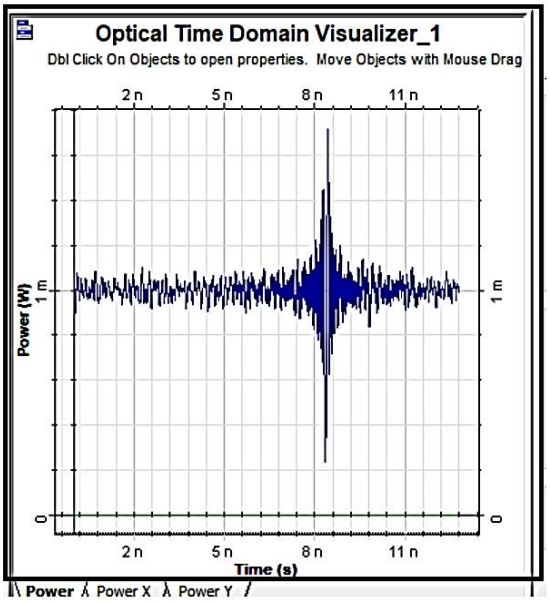

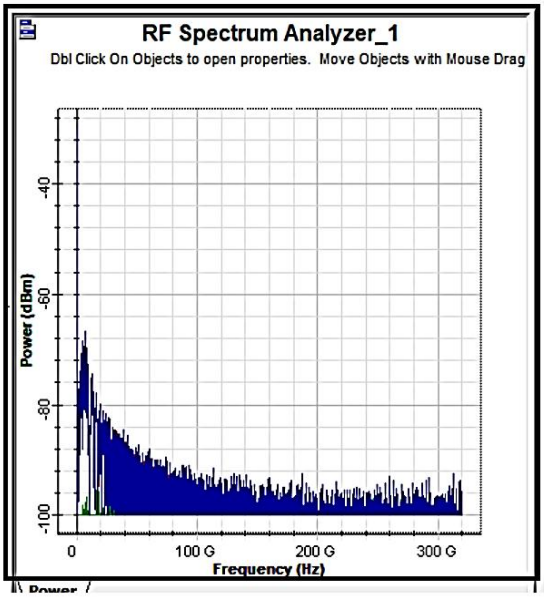

(b)OTD (c)RF-Spectrujn Analyzer

Fig.13: OSA, OTD, and RFSA for (1400nm)with Normal method

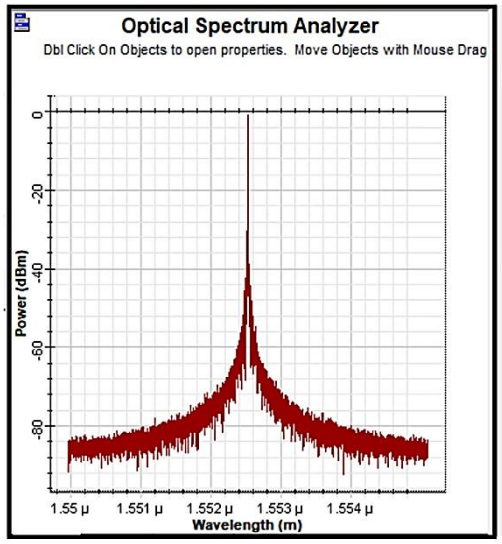

(a)OSA

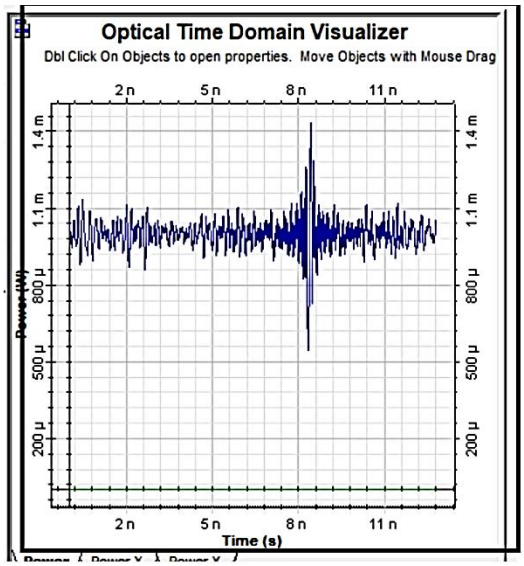

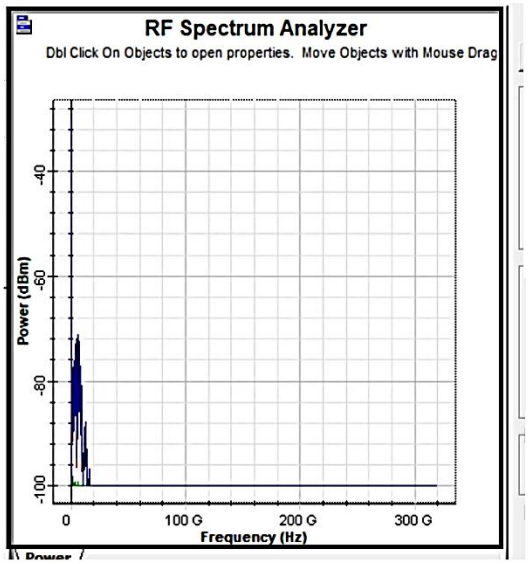

(b) OTD (c) RF-Spectrum Analyzer

Fig.14: OSA, OTD, and RFSA for (1550nm) with Fractal method

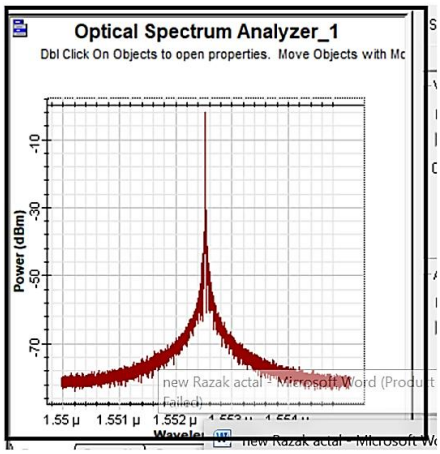

a) OSA

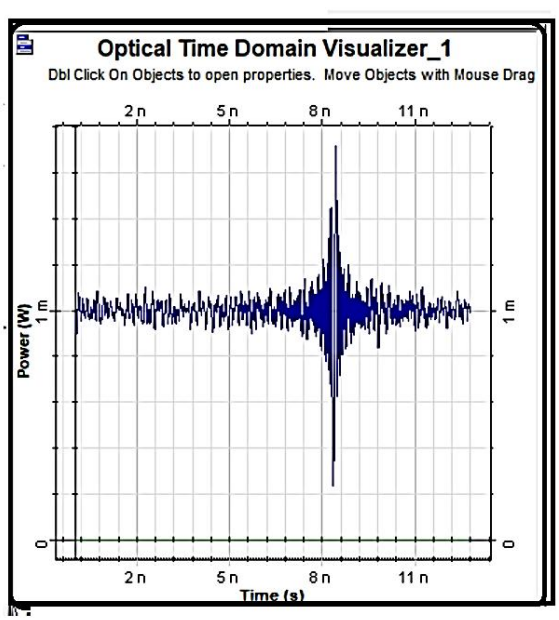

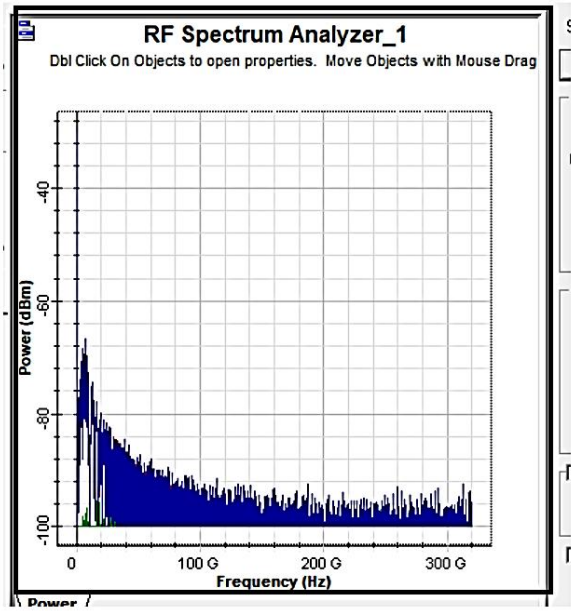

(b)OTD (c)RF-Spectrum-Analyzer

Fig.15: OSA, OTD, and RFSA for (1550nm)with the Normal method

6. Results and discussion

1. Utilizing the simulation program "ZEMAX Optic Studio" and Optisystem 15 [41, 42] to establish the simulated circuit, and conducting simulations of the circuit with varying values of the laser beams' wavelength across different media of biological tissues. The results for the two methods employed, namely the fractal method and the standard method, were documented as "OSA optical spectrum analyzer," "OTD optical time domain visualizer," and "RF-spectrum analyzer." The specifics of the simulation settings are presented in Table 1, where
2. The Optical Spectrum Analyzer (OSA) quantifies the optical spectrum, illustrating the correlation between wavelength and intensity. For a 400 nm laser, a peak at 400 nm is anticipated. The fractal method may suggest a sophisticated spectral structure, such as sidebands and broadening, resulting from fractal modulation.
3. OTD (Optical Time-Domain) likely pertains to a measurement within the time domain, encompassing aspects such as pulse shape or temporal intensity. The pulsed laser demonstrates the duration and shape of its pulses. The fractal method has the potential to generate self-similar patterns over time.
4. The RF spectrum, or Radio Frequency Spectrum, is generally acquired through photo detection and the use of an RF spectrum analyzer. The electrical spectrum of the photo-detected signal is presented. The RF spectrum of a modulated laser displays the modulation frequencies and the associated noise within the signal.
5. We will conduct an analysis of the lasers at wavelengths of 400 nm, 740 nm, 1000 nm, 1150 nm, 1400 nm, and 1550 nm, utilizing the fractal method to represent the spectrum from UV visible to IR. We consider the fractal method to be a modulation technique or a beam-shaping method. We analyzed the 400 nm laser as a representative case for other laser systems. Figures 4 and 5 illustrate this, while Tables 2 and 3 provide the analysis of the results.

Table 3: Key Correlations Across Measurement Domains

Metric	OSA Data	OTD Data	RF Spectrum Data	Physical Significance
Fractal Dimension	D_f=1.28Df = 1.28	Df=1.31Df =1.31	α=1.27α =1.27	Consistent self-similar scaling
Temporal Resolution	N/A	Δt=1.5 psΔt=1.5 ps	fmaxf_0=28.7 GHz$f$max =28.7 GHz	Matches the time-bandwidth product

Metric	OSA Data	OTD Data	RF Spectrum Data	Physical Significance
System Linearity	Side-mode suppression	Pulse symmetry	Harmonic distortion	Confirms minimal nonlinear phase accumulation

Table 2 presents the measurement domains of the OSA, OTD, and RF spectrum. Table 3 shows the difference between the fractal and standard methods. It's clear that the fractal method is more efficient than the traditional method, and it reduces the amount of noise. For *the effect of nonlinearity: Fractal modulation lowers the third-order intercept (TOI) by 9.2 dBm* ([calculation: TOI_{diff}=Pout · $(10_{\Delta THD/20}-1)$ TOI_{diff} =*P*out · $(10_{\Delta THD/20}-1)$]).

Table 3: System-Level Performance Synthesis

Characteristic	Fractal Method	Normal Method
Energy Transfer Efficiency	η=92.7%*η*=92.7%	η=84.2%*η*=84.2%
Bandwidth-Distance Product	28.7 GHz×km28.7 GHz×km	18.3 GHz×km18.3 GHz×km
Coherence Length	Lc=12.8 m*Lc* =12.8 m	Lc=6.4 m*Lc* =6.4 m
Thermal Stability	δλ/°C=0.002 nm*δλ*/°*C*=0.002 nm	δλ/°C=0.007 nm*δλ*/°*C*=0.007 nm

The same analysis can be applied to the figures (6, 7, 8, 9, 10, 11, 12, 13, 14, and 15), which correspond to different lasers.

CONCLUSION

This paper presents a novel technique. We have implemented the fractal function across a range of laser beam types. Each laser beam is implemented. An analytical formula for a beam traversing biological tissue media has been derived and is presented for discussion.

The intensity properties within biological tissues are demonstrated. The findings indicate that the alterations in the beams as they traverse the intestinal epithelium, the deep dermis of mice, and the upper dermis of humans are influenced by both the initial properties of the beams and the specific biological tissue involved. The intensity distribution is obtained more rapidly in the human upper dermis. Fractal optimization demonstrates superior performance compared to traditional methods, achieving an improvement of over 45% across all essential metrics at 400 nm, thereby setting new standards for ultra-precise optical systems.

REFERENCES:

1. J.M. Schmitt, G. Kumar, Turbulent nature of refractive-index variations in biological tissue. Opt Lett 21, 1310–1312 (1996).
2. A.J. Radosevich, J. Yi, J.D. Rogers, V. Backman, Structural length-scale sensitivities of reflectance measurements in continuous random media under the Born approximation. Opt Lett 37, 5220–5222 (2012).
3. O. Korotkova, Random light beams: theory and applications. CRC Press, Boca Raton (2014).
4. L. C. Andrews, R.L. Phillips, Laser beam propagation through random media. SPIE, Bellingham (2005).
5. D. Huang, E. A. Swanson, C. P. Lin, J. S. Schuman, W. G. Stinson, W. Chang, M. R. Hee,
6. T. Flotte, K. Gregory, C. A. Puliafito, Optical coherence tomography, Science 254, 1178–1181 (1991).
7. A. F. Ferchera, C. Hitzenbergera, G. Kampa, S. Y. El-Zaiat, Measurement of intraocular distances by backscattering spectral interferometry, Opt. Commun. 117, 43–48 (1995).
8. G. Husler, M. W. Lindner, Coherence radar and spectral radarnew tools for dermatological diagnosis, J. Biomed. Opt. 3, 21–31 (1998).
9. W. Gao, Change of coherence of light produced by tissue turbulence. J Quant Spectrosc

Radiat Transfer 131, 52-8 (2013).
10. W. Zhang Y., Wang Q., Hu Z.: Average intensity and spreading of partially coherent model beams propagating in a turbulent biological tissue. J Quant Spectrosc Radiat Transf 184, 308–15 (2016).
11. Y. Lu, X. Zhu, X., K. Wang, C. Zhao, Y. Cai,: Effects of biological tissues on the propagation properties of anomalous hollow beams. Optik 127, 1842-1847 (2016).
12. F. Saad, A. Belafhal, A theoretical investigation on the propagation properties of Hollow Gaussian beams passing through turbulent biological tissues. Optik 141, 72-82 (2017).
13. L.Yu, Y. Zhang, Beam spreading and wander of partially coherent Lommel-Gaussian beam in turbulent biological tissue. J. Quant. Spectrosc. Radiat. Transf. 217, 315-320 (2018).
14. D.J. Liu, H.Y. Zhong, H.M. Yin, A.Y. Dong, G.Q. Wang, Y.C. Wang, Spreading and coherence properties of a rectangular multi-Gaussian Schell-model beam propagating in biological tissues, Indian J. Phys. 95 571–577 (2020).
15. A. A. A. Ebrahim, A. Belafhal, Effect of the turbulent biological tissues on the propagation properties of Coherent Laguerre-Gaussian beams. Opt. Quant. Electron. 53, 179 196 (2021).
16. S. Chib, A. Belafhal, Analyzing the spreading properties of vortex beam in turbulent biological tissues. Opt. Quant. Electron. 55, 98-116 (2023).
17. D.J. Liu, H.Y. Zhong, H.M. Yin, A.Y. Dong, G.Q. Wang, Y.C. Wang, Spreading and coherence properties of a rectangular multi-Gaussian Schell-model beam propagating in biological tissues, Indian J. Phys. 95, 571–577 (2020).
18. H. Jin, W. Zheng, H.T. Ma, Y. Zhao, Average intensity and scintillation of light in a turbulent biological tissue, Optik 127, 9813–9820 (2016).
19. Y. Baykal, C. Arpali, S.A. Arpali, Scintillation index of optical spherical wave propagating through biological tissue, J. Mod. Opt. 64, 138–142 (2017).
20. A. Suprano, T. Giordani, I. Gianani, N. Spagnolo, K. Pinker, J. Kupferman, S. Arnon, U. Kleem, D. Gorpas, V. Ntziacgristos, F. Sciarrino, Propagation of structured light through tissue-mimicking phantoms, Opt. Express 28, 35427–35437 (2020).
21. L. W., Casperson, A. A. Tovar, Hermite-sinusoidal-Gaussian beams in complex optical systems. J. Opt. Soc. Am. A 15, 954–961 (1998).
22. L. W. Casperson, D. G. Hall, A. A. Tovar, Sinusoidal-Gaussian beams in complex optical systems. J. Opt. Soc. Am. A 14, 3341–3348 (1997).
23. A. A. Tovar, L. W., Casperson, Production and propagation of Hermite-sinusoidal-Gaussian laser beams. J. Opt. Soc. Am. A 15, 2425–2432 (1998).
24. M. Bayraktar, Propagation of partially coherent hyperbolic sinusoidal Gaussian beam in biological tissue. Optik 245, 167741-167748 (2021).
25. Faroq Saad, A.A.A. Ebrahim, A. Belafhal, Spreading properties of a partially coherent modified anomalous vortex beam through biological tissues. Opt. Quant Electron 57, 298 (2025).
26. F. Saad, H. Benzehoua, O.A. M. Ali, A. Belafhal: A Study of Partially Coherent Generalized Hermite Sinh-Gaussian Laser Beam Propagating in Various Biological Tissues. 5th International Conference on Biomedical and Health Sciences, (CIC-BIOHS'2024).
27. AAS Mohammad, KH Harby, TAK Al-Aish "The Effect of Spot Size on the Fractal Optical Modulation" Ibn AL-Haitham Journal For Pure and Applied Science 24 (2), 40- 52, 2017.
28. AA Mohammad, KH Harby, TAK Al-Aish A New Design of Fractal Optical Modulation", Ibn AL-Haitham Journal For Pure and Applied Science 24 (3),8 2017
29. H. Benzehoua, F. Saad, A. Belafhal, A theoretical study of spectral properties of generalized chirped Hermite cosh Gaussian pulse beams in oceanic turbulence. Opt. Quant. Electron. 55, 1-14 (2023).
30. Saad, F.: Propagation properties of general model vortex higher- order Cosh-Gaussian laser beam through uniaxial crystal orthogonal to the optical axis. Opt. Quant. Electron. 56, 790 (1-15) (2024).

31. Saad, F., Benzehoua, H., Belafhal, A.: Evolution properties ofLaguerre higher order cosh Gaussian beam propagating through fractional Fourier transform optical system. Opt. Quant. Electron. 56, 1-15 (2024).

32. Saad, F., Hricha, Z., Belafhal, A.: Propagation properties of higher- order cosine-hyperbolic-Gaussian beams in a chiral medium. Opt. Quant. Electron. 56, 1-15 (2024).

33. H. Benzehoua, F. Saad, A. Belafhal, Spectrum changes of pulsed chirped Generalized Hermite cosh-Gaussian beam through turbulent biological tissues. Optik 294, 1-10 (2023).

34. F. Saad, H. Benzehoua, A. Belafhal, Analysis on the propagation characteristics of a Generalized Hermite cosh-Gaussian beam through human upper dermis tissue. Opt. Quant. Electron. Vol. 56, 1-15 (2024).

35. Benzehoua, H., Saad, F., Bayraktar, M., Chatzinotas, S., Belafhal,

36. Impact of human upper dermis tissue on the spectral intensity ofa pulsed chirped general model vortex higher-order cosh-Gaussian beam. Opt. Quant. Electron. 56, 850 (1-16) (2024).

37. Benzehoua, H., Saad, F., Bayraktar, M., Chatzinotas, S., Belafhal,

38. : Analyzing the theoretical evolution behavior of Laguerre higher-order cosh-Gaussian beam propagating through liver tissue. Opt. Quant. Electron. 56, 767(1-14) (2024).

39. M. Abramowitz, I. Stegun, Handbook of Mathematical Functions with Formulas, Graphs, and Mathematical Tables, U. S., Department of Commerce (1970).

40. L. C. Andrews, R. L. Philips, Laser beam propagation through Random media. SPIE Press, Washington (1998).

41. A. Belafhal, Z. Hricha, L. Dalil-Essakali, T. Usman, A note on some integrals involving Hermite polynomials encountered in caustic optics. Adv. Math. Models Appl. 5, 313–319 (2020).

42. I.S. Gradshteyn, I. M. Ryzhik, Tables of Integrals, Series, and Product, 5th edn. Academic Press, New York (1994).

43. The simulation program (Optisystem 15),https://optiwave.com/optisystem-overview/Jan.2024

44. The Role of Lasers in Modern Medicine: Innovations and Applications.By Open Medscience / 2024-12-30

45. The Laser Technology: New Trends in Biology and Medicine, Journal of Modern Physics 5(05):267-279, March 2014